Atomic and electronic properties of anion vacancies on the (110) surfaces of InP, InAs, and InSb

M. C. Qian,[1] M. Göthelid,[2] B. Johansson,[1,3] and S. Mirbt[1]
[1]*Condensed Matter Theory Group, Department of Physics, Uppsala University, Box 530, SE-751 21 Uppsala, Sweden*
[2]*Materialfysik, Royal Institute of Technology, SE-100 44 Stockholm, Sweden*
[3]*Applied Materials Physics, Department of Materials Science and Engineering, Royal Institute of Technology, SE-100 44 Stockholm, Sweden*

(Received 28 March 2002; revised manuscript received 25 June 2002; published 29 October 2002)

We have performed total-energy density-functional calculations using first-principles pseudopotentials to determine the atomic and the electronic structure of the anion vacancy on the (110) surfaces of InP, InAs, and InSb. An inward relaxation of the three neighboring In atoms next to the anion vacancy is obtained, but the stable atomic structure depends critically on the vacancy charge state. The $+1$ charged vacancy exhibits a nonsymmetric configuration with one rebonded dimer, while both 0 and -1 charged vacancies show a symmetric configuration with loosely rebonded and rebonded trimer, respectively. For InP and InAs, the charge-transfer levels $\epsilon(+1/0)$ and $\epsilon(0/-1)$ are located around the center of the band gap; whereas for InSb, the -1 charge state is stable in the whole band gap. In contrast to bulk, the surface vacancy is a positive-U center. The band structures and the density of states have been calculated. Three vacancy states, one deep in the valence band and two around the band gap, are identified. Our results show that the character of the vacancy states is mainly dependent on the atomic configuration.

DOI: 10.1103/PhysRevB.66.155326 PACS number(s): 73.20.At, 71.55.Eq, 68.35.Bs

I. INTRODUCTION

The In group-V compound semiconductors are interesting materials with potentially important device applications. When undergoing *n*-type doping, InP is observed to have high electronic mobility and resistance to the rapid mode of laser degradation. InAs and InSb have small band gaps with 0.42 and 0.24 eV, respectively. They are good candidates of useful infrared detectors.[1,2] As intrinsic point defects, surface vacancies play an important role in the growth process of thin semiconductor films and the Fermi-level pinning at metal-semiconductor interfaces. These point defects have been extensively studied by scanning tunneling microscopy (STM) observations and density-functional theory calculations, especially on the GaAs(110) surface.[3] For the As vacancy on the *p*-type GaAs(110) surface, calculations suggest that the two surface gallium atoms neighboring the As vacancy relax into the subsurface layer, while STM experiments observe the presence of two bright spots in the Ga sublattice.[4] It has been well explained via the effect of local-charge-induced band bending by Zhang and Zunger.[5] Furthermore, the charge state of the As vacancy is correctly predicted by the calculations to be $+1$ for *p*-type and -1 for *n*-type GaAs(110). However, the interpretation of the experimental STM images is still unclear. For instance, for the *p*-type GaAs(110) with an As vacancy, one calculation finds that the stable atomic structure is a rebonded configuration breaking the mirror symmetry of the surface,[5] whereas another finds a symmetric configuration to have the lowest energy.[6] Ebert *et al.*[7] argued that the experimentally obtained symmetric STM image is a time average of two degenerate nonsymmetric geometries due to a thermal flip motion between the mirror configurations.

In this paper, we describe a systematic study of the atomic and electronic properties of anion vacancies on the (110) surface of InP, InAs, and InSb. A comprehensive study across this range of materials enables us to understand the observed STM images as well as the character of anion vacancies, especially on the narrow band-gap semiconductor surfaces.

This paper is organized as follows: First, we briefly describe our computational method. In Sec. III, the atomic structures of the anion vacancy surface are presented. In Sec. IV, the vacancy formation energies of the three materials are given. In Sec. V, the nature of the vacancy states is discussed. Finally, we summarize our results.

II. COMPUTATIONAL METHOD

The calculations have been performed using the first-principles total-energy program VASP (Vienna *ab initio* simulation program) (Ref. 8) based on the density-functional theory within local-density approximation.[9] This pseudopotential program uses a plane-wave basis and full nonlocal Vanderbilt-type ultrasoft pseuopotentials to describe the electron-ion interaction. The exchange and correlation potentials are adopted by the functional of Ceperley and Alder as parametrized by Perdew and Zunger.[10] The optimization of the atomic geometry is performed via a conjugate-gradient minimization of the total energy with respect to the atomic coordinates.

To simulate the anion vacancy in the surface, a slab geometry is used with periodic boundary conditions.[11] The supercell contains seven atomic layers with a (2×4) surface unit cell, separated by a 10-Å-thick vacuum layer. The dangling bonds on the bottom surface are passivated by pseudohydrogen.[12] The top four atomic layers are allowed to relax and the equilibrium positions are identified when the forces are smaller than 0.01 eV/Å. A uniform compensating background is incorporated to maintain the charge neutrality of the supercell.

Brillouin-zone integrations have been done on a

Monkhorst-Pack[13] grid of $2\times2\times2$ **k** points, using a smearing of $\sigma=0.05$ eV. The kinetic-energy cutoff of 240 eV is used for the plane-wave basis. The $4d$ electrons of the indium atom are treated as core electrons. All calculations have been performed using the theoretical equilibrium lattice constants of 5.828, 6.013, and 6.430 Å for InP, InAs and InSb, respectively, which are about 0.7% smaller than experimental lattice constants (5.869, 6.036, and 6.479 Å).

III. ATOMIC STRUCTURES

First, using the above computational method, we get the equilibrium geometry of clean (110) surface of In group-V, which we take as a reference. The point group C_{1h} of the surface consists of one mirror plane in the [110] direction. After relaxation, there is a pronounced outward movement of the anions and an inward shift of the cations in the surface layer. The buckling angles are 29.5°, 31.0°, and 32.5°, and the height differences between In and anion are 0.6883, 0.7532, and 0.8507 Å for InP, InAs and InSb, respectively, in good agreement with previous theoretical results[14] and low-energy electron-diffraction data.[15–17] The back bonds of the anion are nearly perpendicular, while the cation shows a planar bonding configuration indicating that the surface anions are p-like bonded and the cations are sp^2-like bonded.

When one anion is removed from the clean (110) surface, an anion vacancy (V_A) is generated. In the following, we discuss the stable structures of anion vacancy. In order to test the dependence of our results on the chosen atomic coordinates, we have tried many starting configurations for most charge states of anion vacancy and found only three different minima.

A. Symmetric configuration

Starting from the unrelaxed anion vacancy surface, after a symmetry-restricted relaxation, the symmetric configuration with an indium trimer [Fig. 1(a)] is obtained for the three materials, regardless of the vacancy charge states.

From Fig. 1(a), we can see that the two surface In atoms neighboring the V_A [In(2) and In(3)] move inward, the subsurface In atom [In(1)] shifts towards the V_A, and the result is a rebonding between the surface and the subsurface In atoms [In(1)-In(2) and In(1)-In(3)]. Because of these new bonds, the coordination number of In(1) is changed to 5. A pyramid encompassing the In(1) atom is formed and the In(1) atom is slightly above the base plane of the pyramid. This local geometry is responsible for the d character of wave function around In(1), which we discuss in Sec. V.

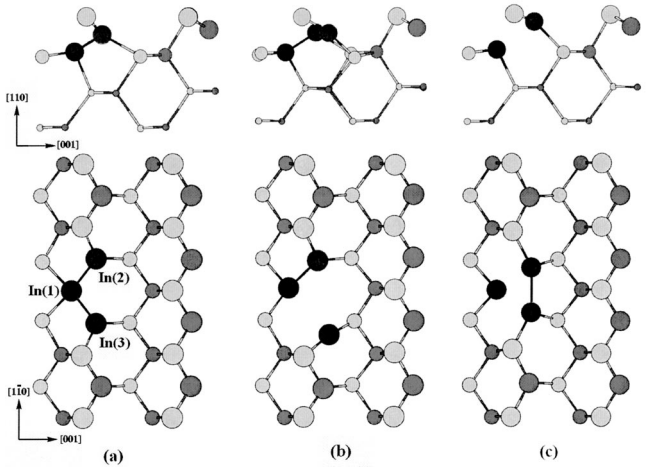

FIG. 1. Side view and top view of the atomic structure with (a) symmetric configuration, (b) nonsymmetric configuration, and (c) symmetric configuration with one loosely rebonded dimer for In group-V (110) surface with anion vacancy. Black circles are for indium atoms and gray circles are for anions. Large, middle, and small radii refer to the surface, subsurface, and bulk atoms.

For the three charge states of the vacancy, i.e., V_A^{+1}, V_A^0, and V_A^{-1}, there are somewhat quantitative differences of the ionic relaxation although the atomic structures are similar. After relaxation, only the nearest neighbors around the V_A are significantly relaxed and all other atoms remain close to the ideal position of a clean surface with a maximum relaxation smaller than 0.15 Å. We summarize the calculated ionic relaxation in Table I and the changes of interatomic distances in Table II for the three materials. As the number of electrons trapped at the vacancy site increase, the surface In(2) and In(3) ions relax further towards the vacancy site along both the [001] and [110] directions, and the subsurface In(1) ion also moves further towards the vacancy site. The negative sign of $\Delta[1\bar{1}0]$ denotes that the surface indium atoms In(2) and In(3) move away from each other in the [110] direction,

TABLE I. Relaxations of the nearest-neighbor In atoms of the $+1$, 0, and -1 charged anion vacancies on the In group-V(110) surface with symmetric configuration from the ideal position of clean surface. The positive sign denotes the relaxation towards the vacancy site. $\|\Delta\|$ is the total displacement. All values are given in angstroms. Atomic indices are same as in Fig. 1.

		$(+1)$				(0)				(-1)			
		[001]	[110]	[110]	$\|\Delta\|$	[001]	[110]	[110]	$\|\Delta\|$	[001]	[110]	[110]	$\|\Delta\|$
InP	In(1)	0.30	0.00	0.08	0.31	0.36	0.00	0.14	0.39	0.50	0.00	0.19	0.54
	In(2)	0.18	−0.09	0.27	0.34	0.31	−0.04	0.31	0.44	0.38	−0.06	0.34	0.51
InAs	In(1)	0.37	0.00	0.14	0.40	0.49	0.00	0.18	0.52	0.61	0.00	0.24	0.65
	In(2)	0.21	−0.10	0.29	0.37	0.31	−0.05	0.34	0.46	0.42	−0.09	0.37	0.57
InSb	In(1)	0.57	0.00	0.24	0.62	0.65	0.00	0.25	0.70	0.75	0.00	0.28	0.80
	In(2)	0.39	−0.01	0.37	0.54	0.45	−0.02	0.42	0.61	0.49	−0.04	0.45	0.67

TABLE II. Interatomic distances (in angstroms) between three indium atoms around the $+1$, 0, and -1 charged anion vacancies with symmetric atomic configuration. Atomic indices are same as in Fig. 1.

	InP			InAs			InSb		
	$(+1)$	(0)	(-1)	$(+1)$	(0)	(-1)	$(+1)$	(0)	(-1)
d_{12}	3.160	2.969	2.836	3.150	2.964	2.834	3.027	2.935	2.861
d_{23}	4.304	4.195	4.241	4.172	4.369	4.425	4.570	4.581	4.624

while the subsurface In(1) does not shift in this direction due to the symmetry. As a result, the trimer bond length d_{12} (d_{13}) is decreased, and finally reaches the indium dimer bond length for the -1 charge state, i.e., 2.836, 2.834, and 2.861 Å for InP, InAs, and InSb, respectively. The atomic distance d_{23} does not change very much and is kept relatively large, indicating the antibonding character between surface In(2) and In(3) ions, regardless of the charge state of the vacancy.

B. Nonsymmetric configuration

In order to obtain the other possible configuration, we move one surface indium atom off the ideal position of the unrelaxed anion vacancy surface by 2% of the lattice constant in both [001] and [110] directions. Starting from this configuration, when we perform the symmetry-unrestricted calculations for the anion vacancy on the (110) surface of InP, InAs, and InSb, the mirror symmetry of the surface is broken by the ionic relaxation around the vacancy for both V_A^{+1} and V_A^{-1}, but it is kept for the neutral vacancy V_A^0. Other starting configurations are tested to give the same results. Our results are consistent with the previous calculations of the As vacancy on the GaAs(110) surface by Zhang and Zunger[5] and Ebert *et al.*,[7] but different to the symmetry-conserving result by Kim and Chelikowsky.[6]

The nonsymmetric configuration is shown in Fig. 1(b). One of the surface indium ions [In(2)] forms a dimer with the subsurface In(1) ion. Another surface indium ion [In(3)] is relaxed to become twofold coordinated. The detailed ionic relaxations are listed in Table III and the interatomic distances are listed in Table IV. The subsurface In(1) moves toward the vacancy site only in the [001], [110] plane, but almost not in the [110] direction. One surface indium neighbor atom [In(2)] moves inward in the three directions to dimerize with In(1), while the other indium neighbor atom [In(3)] moves away. In the [110] direction, In(3) moves inward for the $+1$ charged vacancy and outward for the -1 charged vacancy.

For different charged vacancies V_A^{+1} and V_A^{-1}, the indium rebonded dimer bond length d_{12} is almost the same. However, when two electrons are added into the vacancy site, the second vacancy state (mainly derived from the three neighboring In atoms) becomes occupied, and thus both the interatomic distances d_{13} and d_{23} decrease going from V_A^{+1} to V_A^{-1} (see Table IV), which indicates stronger bonds between the indium atoms when additional electrons occupy the vacancy state.

TABLE III. Relaxations of the nearest-neighbor In atoms of the $+1$ and -1 charged anion vacancy on the In group-V(110) surface with nonsymmetric configuration from the ideal position of clean surface. The positive sign denotes the relaxation towards the vacancy site. $\|\Delta\|$ is the total displacement. All values are given in angstroms. Atomic indices are same as in Fig. 1.

		$(+1)$				(-1)			
		[001]	[110]	[110]	$\|\Delta\|$	[001]	[110]	[110]	$\|\Delta\|$
InP	In(1)	0.18	0.15	0.03	0.24	0.14	0.15	−0.04	0.21
	In(2)	0.41	0.15	0.27	0.51	0.30	0.56	0.11	0.65
	In(3)	−0.37	−0.85	0.29	0.97	−0.23	0.48	−0.50	0.73
InAs	In(1)	0.20	0.21	0.06	0.29	0.13	0.17	−0.05	0.22
	In(2)	0.45	0.12	0.28	0.54	0.36	0.59	0.15	0.70
	In(3)	−0.43	−0.96	0.24	1.08	−0.18	0.54	−0.49	0.75
InSb	In(1)	0.24	0.28	0.06	0.38	0.19	0.19	−0.04	0.28
	In(2)	0.57	0.16	0.35	0.69	0.41	0.73	0.19	0.86
	In(3)	−0.44	−1.11	0.31	1.24	−0.09	0.72	−0.44	0.85

We do not totally agree with the comment on the symmetry of the geometry by Kim and Chelikowsky.[6] Our adopted energy cutoff and surface unit cell are enough for the convergence of relaxation. We test that higher energy cutoff and larger surface unit cell do not modify our results. It is true that the dispersion of vacancy-associated band is larger with the lower energy cutoff and the smaller size of the surface unit cell because of the vacancy-vacancy interaction, especially in the [110] direction. However, it should not be related with the symmetry breaking. In fact, for the $+1$ charged vacancy, two electrons occupy one vacancy state arising from one rebonded dimer and a nonsymmetric configuration with the distortion is preferable. For the -1 charged vacancy, four electrons occupy two vacancy states from the rebonded trimer and a symmetric configuration is favorable. The above qualitative conclusions are proven by the total-energy calculations described in the following section.

C. Symmetric configuration with one loosely rebonded dimer

It is interesting that if we start from the unrelaxed anion vacancy surface but with two surface indium ions closer to each other, a second symmetric configuration is metastable only for the -1 charged vacancy, as shown in Fig. 1(c). In this configuration, two surface In atoms loosely rebond and move away from the vacancy site. We only list the interatomic distances in Table V. The loosely-rebonded indium dimer bond length is almost the same for all three materials and slightly larger than the indium dimer bond length.

IV. VACANCY FORMATION ENERGY

The formation energy of an anion vacancy in charge state q (V_A^q) depends on the chemical potential μ_A, of the anion, and the surface Fermi level[18] ϵ_f (measured from the valence-band maximum ϵ_{VBM}):

$$E_f(\mu_a, q) = E_{tot}^{LDA}(q) - E_{tot}^{LDA}(\text{slab}) + \mu_A + q(\epsilon_{VBM} + \epsilon_f),$$

TABLE IV. Interatomic distances(in angstroms) between three indium atoms around the $+1$ and -1 charged anion vacancy with nonsymmetric atomic configuration. Atomic indices are same as in Fig. 1.

	InP		InAs		InSb	
	$(+1)$	(-1)	$(+1)$	(-1)	$(+1)$	(-1)
d_{12}	2.861	2.845	2.870	2.852	2.877	2.867
d_{13}	4.238	3.725	4.486	3.749	4.826	3.743
d_{23}	4.887	3.186	5.172	3.238	5.593	3.196

where $E_{tot}^{LDA}(q)$ $[E_{tot}^{LDA}(\text{slab})]$ is the total energy of the (110) surface with (without) a vacancy.

Normalizing the formation energy with respect to the neutral vacancy, the formation energy can be written as

$$E_f(q/0) = E_{tot}^{LDA}(q) - E_{tot}^{LDA}(0) + q(\epsilon_{VBM} + \epsilon_f).$$

Figure 2 shows the calculated formation energy of the anion vacancies on the (110) surface of InP, InAs, and InSb, as a function of the Fermi level which varies from the valence-band maximum (VBM) to the calculated conduction-band minimum (CBM). On the *p*-type InP(110) surface, the $+1$ charge state of the *P* vacancy is stable, which is in accord with two recent experimental results using the compensation of local band bending between the vacancy[19] and the *p*-type dopant and through a statistical analysis of the vacancy distribution.[20] On the *n*-type InP(110) surface, the -1 charged state of the *P* vacancy is stable. The neutral state is stable only in a narrow energy range. Our calculated charge-transfer levels are $\epsilon(+1/0)$ at 0.388 eV and $\epsilon(0/-1)$ at 0.576 eV, for the calculated band gap of 1.11 eV. Ebert *et al.*[7] combined STM and photoelectron spectroscopy experiments to determine the charge-transfer level $\epsilon(+1/0)$ of the *P* vacancy and measured it to be 0.75 eV above VBM at room temperature. In addition, they calculate the charge-transfer level $\epsilon(+1/0)$ to be 0.52 eV for the calculated band gap of 1.26 eV. The discrepancy is within the error bar of the theoretical calculations.[21]

On the InAs(110) surface, the stable charge states of the As vacancy are the same as for the *P* vacancy on InP(110), i.e., -1 for *p*-type InAs and $+1$ for *n*-type InAs. The charge-transfer levels $\epsilon(+1/0)$ and $\epsilon(0/-1)$ are located at 0.20 eV and 0.277 eV. They are located around the center of the energy gap. However, on the InSb(110) surface, the -1 charged state of the Sb vacancy is stable in the whole energy gap. It will be discussed in the following section from the electronic structure of InSb(110) surface with Sb vacancy. In all the three materials, multiple charge states of the anion vacancy are unfavorable. Our calculated charge state of the anion vacancy is consistent with the observed STM results that the anion vacancies on *n*-type InP, InAs, and InSb(110) surfaces are negatively charged.[22–24]

We now focus on the energetically stable atomic structure of the V_A on the (110) surface. For the $+1$ charged vacancy V_A^{+1}, the total energy of the nonsymmetric configuration is 75, 124, and 100 meV lower than the symmetric configuration in the (110) surface of InP, InAs, and InSb, respectively. In contrast, for the -1 charged vacancy V_A^{-1}, the nonsymmetric configuration is higher by 88, 298, and 443 meV than the symmetric configuration of the (110) surface of InP, InAs, and InSb, respectively. For the neutral anion vacancy V_A^0, the symmetric configuration with the loosely rebonded trimer has the lowest energy. Combining the stable charge states of the vacancy with the formation energies, we find for the anion vacancies on the *p*-type InP and InAs(110) surfaces, the nonsymmetric configuration to be energetically

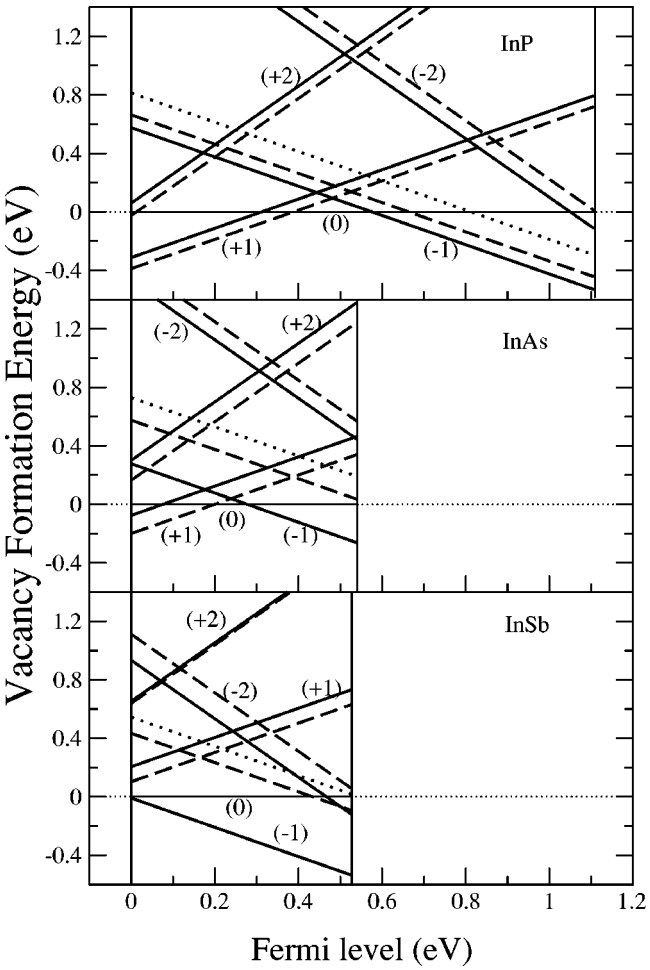

FIG. 2. Fermi-level dependence of the formation energy $E_f(q/0)$ of different charged anion vacancy on the (110) surface. Solid, dashed, and dotted lines denote the symmetric, nonsymmetric, and one loosely rebonded dimer symmetric configurations. The symbols denote the charge state of the vacancy. The reference of Fermi level is the valence-band maximum. The right vertical line refers to the calculated conduction-band minimum.

TABLE V. Interatomic distances (in angstroms) between three indium atoms around the anion vacancy for the -1 charge state of symmetric atomic configuration with one loosely rebonded dimer. The atomic indices are same as in Fig. 1.

	InP	InAs	InSb
d_{12}	3.153	3.159	3.161
d_{23}	2.941	2.952	2.946

most stable; for the anion vacancies on the *n*-type InP and InAs(110) surfaces, the symmetric configuration is the most stable; for both the *p*-type and the *n*-type InSb(110) surface, the Sb vacancy shows a stable symmetric configuration.

In contrast to bulk,[25] the surface anion vacancy is a positive-U center, in which the charge state as a function of the Fermi level can be either $+1$, 0, or -1. Considering the electronic transition $(0/-1)$, the initial state is the relaxed neutral charge state of the vacancy V_A^0, the intermediate state is the unrelaxed -1 charged state of the vacancy V_A^{-1}, and the final state is the relaxed -1 charged state of the vacancy V_A^{-1}. The so-called Franck-Condon shift[27] or the relaxation energy E_{FC} is calculated from the energy difference between the unrelaxed and relaxed configuration of the -1 charged vacancy, which amounts to 0.13, 0.13, and 0.06 eV for InP, InAs, and InSb, respectively. The surface relaxation energies are approximate half of the bulk counterparts.[26] The energy lowering due to the lattice relaxation is less than the inter-electron Coulomb interaction. We use the Franck-Condon formula $\Delta E = -E_{FC} + U$ to estimate the on-site Coulomb interaction around the vacancy site. ΔE can be obtained from the difference between the $\epsilon(+1/0)$ and $\epsilon(0/-1)$ transfer levels. The calculated value of U is 0.3, 0.2, and 0.1 eV for the P, As, and Sb vacancy, respectively.

V. VACANCY STATES

The surface band structures of the $+1$ charged anion vacancy on the (110) surface of InP, InAs, and InSb are shown in Figs. 3–5 for both the symmetric and nonsymmetric configurations. The triangles represent the vacancy states whose weight projected on the three neighboring In atomic sites is larger than 30% of the whole squared modulus of the wave function. The full dots are used for the states localized at the surface. These are defined as those states whose squared modulus integrated over the top layer exceeds 0.25. (If a state is equally distributed over all layers, whose weight in the top layer amounts to $1/7 = 0.143$.) There are three bands associated with the vacancy site, which are referred to as vacancy state α, β, and γ. We do not show the vacancy state α in the figures as it is a very flat band, deep inside the valence-band complex, located near the upper edge of the lower gap and related to the strong atomic relaxation around the V_A. The nature of the two other vacancy states changes with the materials as well as with the configurations. The following characteristics can be given:

(i) Apart from the vacancy states, the valence bands of the three materials are similar, because these three materials have the same zinc-blende structure and similar chemical bonding. However, the conduction band varies from one material to another. In particular, the conduction-band edge around the Γ point in InAs, like the clean surface, has a sharp well.

(ii) The vacancy states β and γ are located around the band gap. Their exact energy position determines which charge state becomes stable when the Fermi level is shifted from VBM to CBM.

(iii) Focusing on the symmetric configuration, the bands of the vacancy state β are similar for the three materials, which indicates that the vacancy state β hybridizes with the localized surface states derived from the valence states.

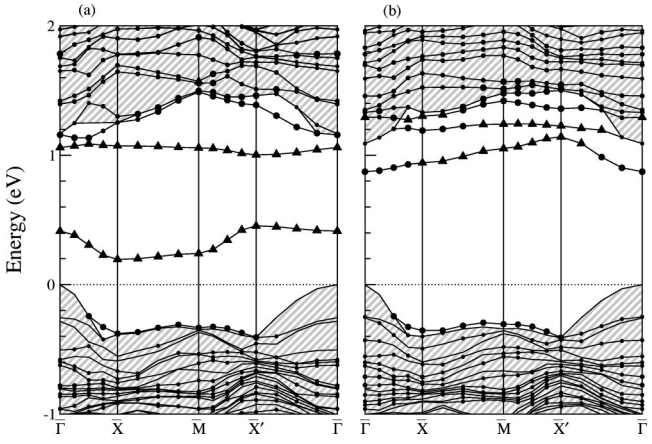

FIG. 3. Band structures for the $+1$ charged P vacancy on the InP(110) surface with (a) symmetric configuration and (b) nonsymmetric configuration. High-symmetry points of the surface Brillouin zone are $\overline{\Gamma}=(0,0)$, $\overline{X}=(0,1)$, $\overline{M}=(1,1)$, and $\overline{X'}=(1,0)$. The valence-band maximum is set as the zero energy. The triangles represent the vacancy states. See text for the details.

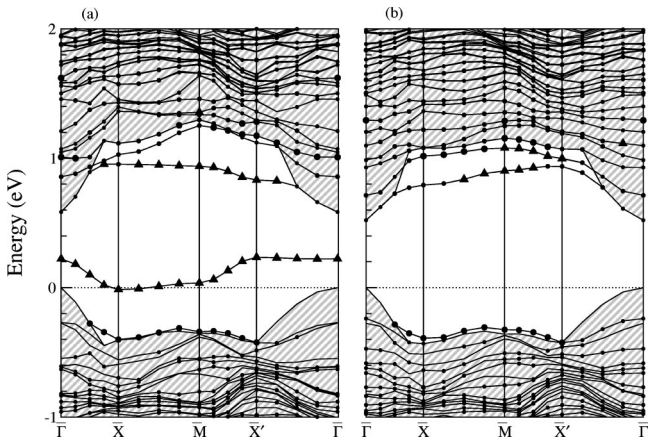

FIG. 4. Same as Fig. 3, but for the InAs(110) surface.

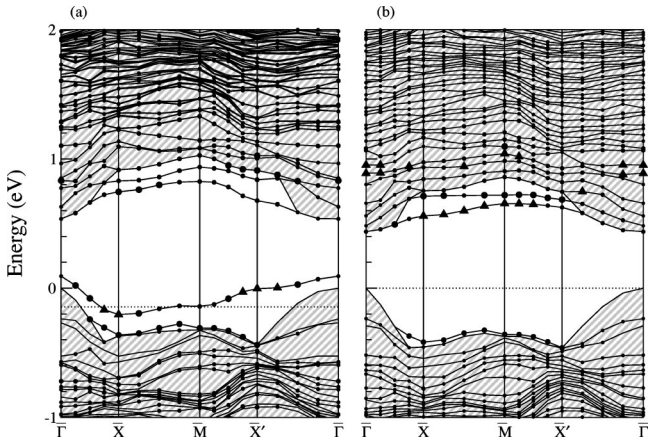

FIG. 5. Same as Fig. 3, but for the InSb(110) surface.

However, the bands of the vacancy state γ are quite different from each other, due to the hybridization with the localized surface states derived from the conduction states. The vacancy state β has a flat band along $\bar{\Gamma}$-$\bar{X}'$ ([001] direction), but a dispersive band along $\bar{\Gamma}$-$\bar{X}$ ([$\bar{1}$10] direction). For InP and InAs, they are located around the band gap and relatively close to the VBM, but for InSb it goes below the VBM. The bandwidth of the vacancy state β with 0.20, 0.23, and 0.29 eV follows the on-site U value, i.e., it increases from InP, InAs to InSb.

(iv) For nonsymmetric configuration, both the vacancy states β and γ move upward, especially the bands of the state β change very much, compared with one of the symmetric configuration. In InAs, the vacancy state β are deep into the conduction band, which should not affect the character of the conduction-band edge.

(v) Among the three materials, the vacancy states β and γ of InSb show the strongest hybridization with the localized surface states derived from the valence states and the conduction states, respectively. Because the vacancy state β of InSb is below the VBM, it is always occupied to reduce the total energy when the Fermi level is shifted from VBM to CBM. The Sb vacancy shows -1 charge state, even for the p-type InSb.

In Figs. 6–8, we give the total density of state (DOS) and partial DOS (projected on the three In atoms around the $+1$ charged vacancy) for both the symmetric and nonsymmetric configurations. There are three peaks labeled α, β, and γ in the total DOS. For the symmetric configuration, the vacancy state α is distributed around the three In atoms and has mainly s character. The vacancy state β mainly from the three In atoms has p character. Apart from that, the relatively small contribution from the subsurface In(1) has d character due to the local geometry. The vacancy state γ has p_π character and is distributed over the two surface In atoms. For the nonsymmetric configuration, the nature of the vacancy states is quite different. The vacancy state α comes from the indium dimer atoms [In(1) and In(2)] and has s character. The vacancy state β is mainly located on the surface In(3) with p character and in a small part on the dimer atoms In(1), In(2) with p character. Both the β and γ peaks are extensive, indicating the stronger hybridization with the conduction states.

In Fig. 9, we give the modulus of the wave function for the three vacancy states in the InP(110) surface with the $+1$ charged P vacancy, which visibly show the nature of the vacancy states. From Fig. 9(a), it is clear that the vacancy state α is very localized, but the vacancy state β is somewhat dispersive. Most of the charge of the vacancy state β are distributed over the two surface indium atoms with antibonding character. Except that, the charge is located around the surface neighboring anion atomic site along the [110] direction to some extent. For more precise calculations, the surface unit cell in the [110] direction should be increased to reduce the vacancy-vacancy interaction. The vacancy state γ shows the π-bonding character and its spatial distribution above the two surface In atoms is related with the empty image of experimental STM. For the nonsymmetric configuration [Fig. 9(b)], the vacancy state α is localized on the dimer; the vacancy state β has the antibonding character between the surface atom and the dimer; the vacancy state γ is nonsymmetrically distributed over the two surface In atoms.

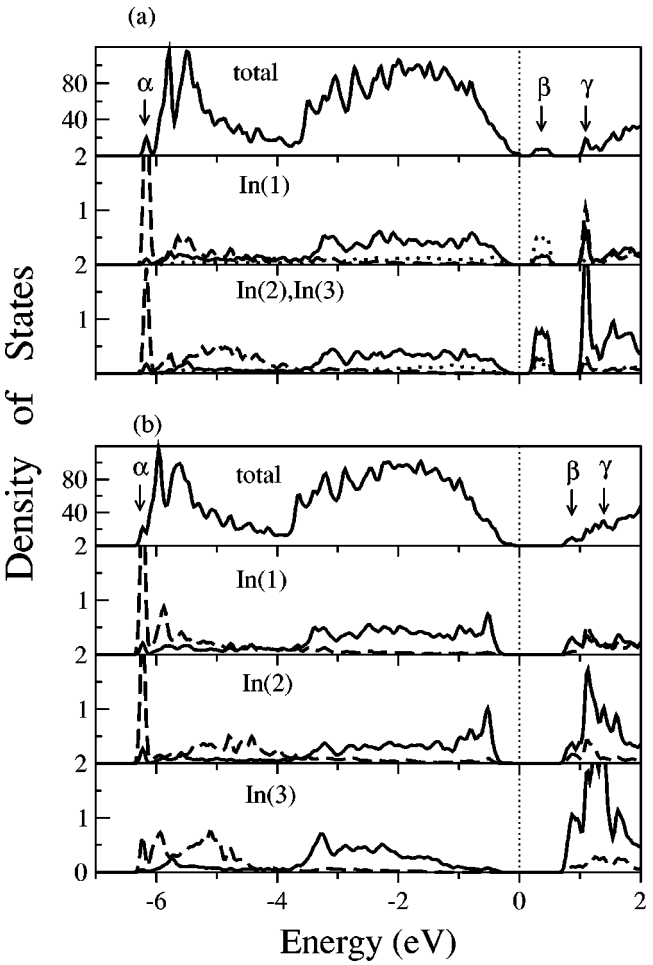

FIG. 6. Total density of states, and the partial density of states on In(1), In(2), and In(3) for the $+1$ charged P vacancy on the InP(110) surface surface with (a) symmetric configuration; (b) nonsymmetric configuration. The dashed, solid, and dotted lines refer to $5s$, $5p$, and $5d$, respectively. Vertical dashed line refers to the Fermi level and the valence-band maximum is set as the zero energy.

The position of the three vacancy states in three charge states for the symmetric configuration are listed in Table VI. Due to the same geometry of the vacancy, there are similar electronic structure for three charge states. The position of three vacancy states are slightly shifted up from V_A^{+1}, V_A^0 to V_A^{-1}. In the $+1$ charged vacancy, state α is fully occupied, state β and γ are fully empty. For the 0 charged vacancy, state β is half occupied, and is fully occupied for the -1 charged vacancy. The vacancy state β is crucial for the electronic property of the material. It is located around the center of band gap for the InP and InAs, but goes below VBM for the InSb, which is related with the stable -1 charged state in a whole band gap.

From the tight-binding point of view, the vacancy states

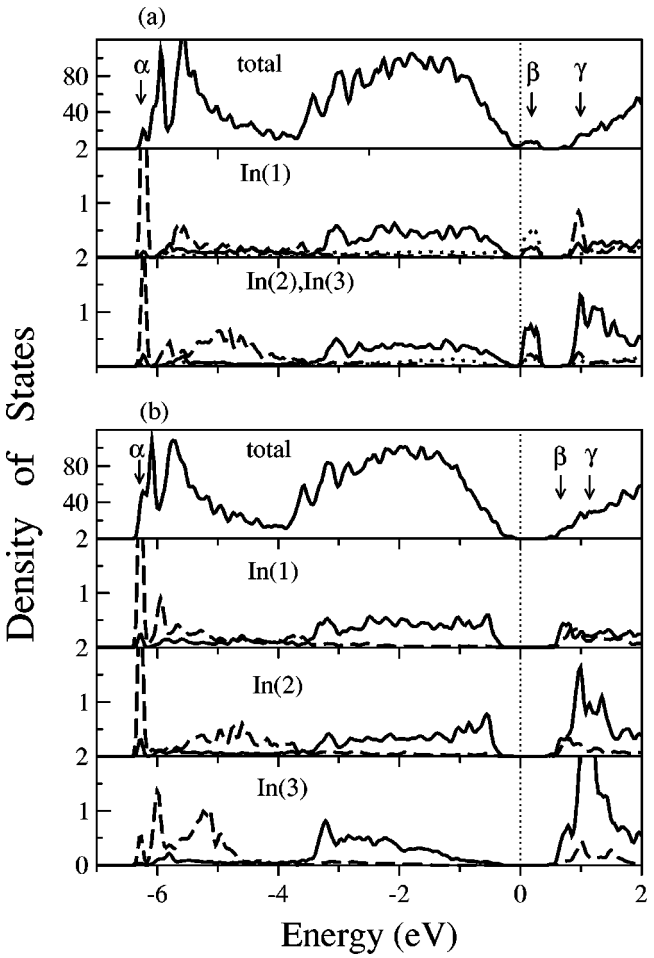

FIG. 7. Same as Fig. 6, but for the InAs(110) surface.

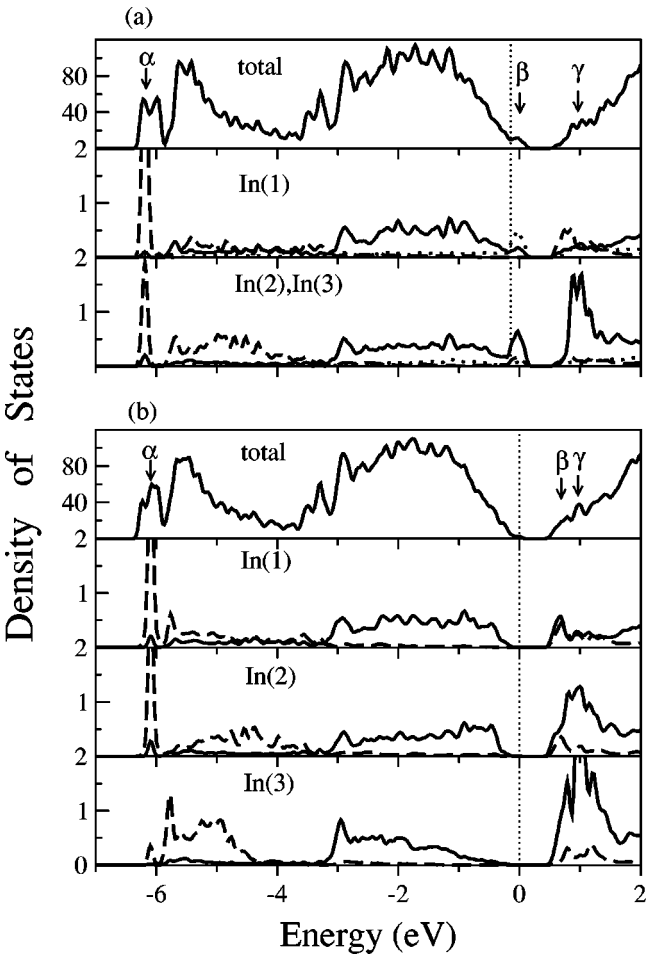

FIG. 8. Same as Fig. 6, but for the InSb(110) surface.

can be regarded as the combination of three atomic orbitals of the surrounding indium atoms.[26] Considering the symmetric configuration, we assumed the three atomic orbitals $\psi_1 = (1\ 0\ 0), \psi_2 = (0\ 1\ 0)$, and $\psi_3 = (0\ 0\ 1)$ and the vacancy wave function $\psi = (a\ b\ c)$. The on-site energy is zero for In(1) and ε_0 for In(2), In(3). The strong interaction between the In(1) and In(2)[In(3)] is $-\varepsilon_1$, and the weak one between the In(2) and In(3) is $-\varepsilon_2$. Therefore, the Hamiltonian is as follows:

$$H = \begin{pmatrix} 0 & -\varepsilon_1 & -\varepsilon_1 \\ -\varepsilon_1 & \varepsilon_0 & -\varepsilon_2 \\ -\varepsilon_1 & -\varepsilon_2 & \varepsilon_0 \end{pmatrix}.$$

By solving the Schördinger equation, the following three eigenvalues and eigenfunctions are obtained:

$$E_\alpha = \frac{1}{2}(\varepsilon_0 - \varepsilon_2) - \frac{1}{2}\sqrt{(\varepsilon_0 - \varepsilon_2)^2 + 8\varepsilon_1^2},$$

$$\psi_\alpha = \left(\frac{1}{2\varepsilon_1}(\varepsilon_0 - \varepsilon_2) + \frac{1}{2\varepsilon_1}\sqrt{(\varepsilon_0 - \varepsilon_2)^2 + 8\varepsilon_1^2} \quad 1 \quad 1 \right),$$

$$E_\beta = \varepsilon_0 + \varepsilon_2, \qquad \psi_\beta = (0 \quad 1 \quad -1),$$

$$E_\gamma = \frac{1}{2}(\varepsilon_0 - \varepsilon_2) + \frac{1}{2}\sqrt{(\varepsilon_0 - \varepsilon_2)^2 + 8\varepsilon_1^2},$$

$$\psi_\gamma = \left(\frac{1}{2\varepsilon_1}(\varepsilon_0 - \varepsilon_2) - \frac{1}{2\varepsilon_1}\sqrt{(\varepsilon_0 - \varepsilon_2)^2 + 8\varepsilon_1^2} \quad 1 \quad 1 \right).$$

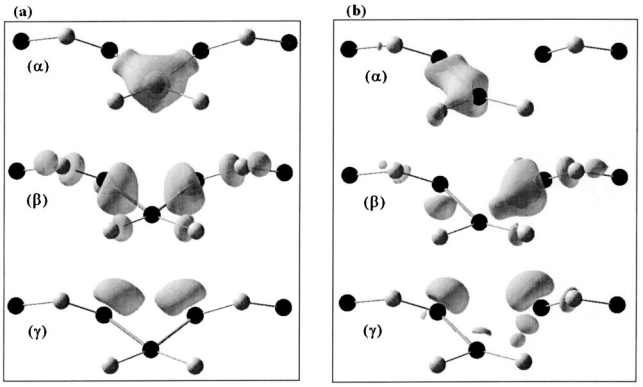

FIG. 9. Perspective view of the isosurface of electron density of the vacancy states α, β, and γ for one positively charged P vacancy on the InP(110) surface with (a) the symmetric configuration and (b) the nonsymmetric configuration. Black circles are for indium atoms and gray circles are for anions. The isosurface value is 0.017 electrons/Å^3.

TABLE VI. The central position of three vacancy states (in eV) for the +1, 0 and −1 charged anion vacancies with symmetric atomic configuration. The valence-band maximum is set as the zero energy.

	InP			InAs			InSb		
	(+1)	(0)	(−1)	(+1)	(0)	(−1)	(+1)	(0)	(−1)
State α	−6.205	−6.066	−5.920	−6.284	−6.196	−6.089	−6.241	−6.215	−6.072
State β	0.326	0.479	0.580	0.119	0.212	0.278	−0.095	−0.031	0.031
State γ	1.095	1.386	1.592	0.936	1.166	1.318	0.843	0.948	1.047

Without loss in generality, we set $\varepsilon_0=2.2$, $\varepsilon_1=1.0$, and $\varepsilon_2=0.2$, the eigenvalues and eigenfunctions are as follows:

$$E_\alpha=-0.73, \quad \psi_\alpha=(2.73 \quad 1 \quad 1),$$

$$E_\beta=2.4, \quad \psi_\beta=(0 \quad 1 \quad -1),$$

$$E_\gamma=2.73, \quad \psi_\gamma=(0.73 \quad 1 \quad 1).$$

The results show that the lowest vacancy state is largely located on the subsurface atom; the second vacancy state is located at the two surface atoms, but with antibonding character; and the third vacancy state mainly comes from the two surface atoms. This simple tight-binding model gives a rather good qualitative understanding of the vacancy states.

VI. SUMMARY

We have investigated the anion vacancy on the In group-V (110) surfaces using *ab initio* pseudopotentials with a plane-wave basis. The atomic relaxation shows that the three nearest-neighbor indium atoms move towards the vacancy site. However, the stable atomic configuration depends critically on the charge state of the vacancy. From the calculation of the vacancy formation energy, we determine that the stable charge state of the vacancy is +1 for *p*-type InP and InAs (110) surfaces, which exhibit a nonsymmetric configuration with one rebonded dimer. In contrast, for *n*-type InP and InAs (110) surfaces the −1 charge state and a symmetric configuration with a rebonded trimer is most stable. The charge-transfer level is located around the center of the energy gap. Therefore, the anion surface vacancy is a compensating center of bulk doping for InP and InAs. However, for both the *p*-type and *n*-type InSb (110) surface, only a −1 charge state of the Sb vacancy is stable in the whole band gap, and the structure has a symmetric configuration with a rebonded trimer. In contrast to bulk, we calculate the surface vacancy to be a positive-U center with a decreasing value of U in the order of InP, InAs, and InSb. By analyzing the band structure and DOS, our results indicate that the nature of the vacancy states is mainly dependent on the atomic geometry.

ACKNOWLEDGMENTS

We thank Christopher Castleton for his helpful discussions and letting us quote his results prior to publication. We are grateful to the Swedish Science Research Council (VR) and Göran Gustafsson Foundation for financial support.

[1] C.A. Hoffman, H.J. Geritsen, and A.V. Nurmikko, J. Appl. Phys. **51**, 1603 (1980).
[2] I. Hayashi, J. Phys. Soc. Jpn. **49**, 57 (1980), and references therein.
[3] Ph. Ebert, Surf. Sci. Rep. **33**, 121 (1999).
[4] G. Lengel, R. Wilkins, G. Brown, M. Weimer, J. Gryko, and R.E. Allen, Phys. Rev. Lett. **72**, 836 (1994).
[5] S.B. Zhang and A. Zunger, Phys. Rev. Lett. **77**, 119 (1996); **79**, 3313 (1997).
[6] H. Kim and J.R. Chelikowsky, Phys. Rev. Lett. **77**, 1063 (1996); Phys. Rev. Lett. **79**, 3315 (1997); Surf. Sci. **409**, 435 (1998).
[7] Ph. Ebert, K. Urban, L. Aballe, C.H. Chen, K. Horn, G. Schwarz, J. Neugebauer, and M. Scheffler, Phys. Rev. Lett. **84**, 5816 (2000).
[8] G. Kresse and J. Hafner, Phys. Rev. B **47**, 558 (1993); **49**, 14 251 (1994); G. Kresse and J. Furthmüller, Comput. Mat. Sci. **6**, 15 (1996); G. Kresse and J. Furthmüller, Phys. Rev. B **55**, 11 169 (1996), and references therein.
[9] W. Kohn and L.J. Sham, Phys. Rev. **140**, A1133 (1965).
[10] J.P. Perdew and A. Zunger, Phys. Rev. B **23**, 5048 (1981).
[11] M. Schlüter, J.R. Chelikowsky, S.G. Louie, and M.L. Cohen, Phys. Rev. B **12**, 4200 (1975).
[12] K. Shiraishi, J. Phys. Soc. Jpn. **59**, 3455 (1990).
[13] H.J. Monkhorst and J.D. Pack, Phys. Rev. B **13**, 5188 (1976).
[14] D.J. Chadi, Phys. Rev. B **19**, 2074 (1979); A.C. Ferraz and G.P. Srivastava, Surf. Sci. **182**, 161 (1987); B. Engels, P. Richard, K. Schroeder, S. Blügel, Ph. Ebert, and K. Urban, Phys. Rev. B **58**, 7799 (1998).
[15] C. Mailhiot, C.B. Duke, and D.J. Chadi, Surf. Sci. **149**, 366 (1985); Phys. Rev. Lett. **53**, 2114 (1984); D.J. Chadi, Phys. Rev. B **19**, 2074 (1979).
[16] A. Kahn, Surf. Sci. Rep. **3**, 193 (1983).
[17] F. Bechstedt and R. Enderlein, *Semiconductor Surfaces and Interfaces* (Akademie Verlag, Berlin, 1988), and references cited therein.
[18] U. Scherz and M. Scheffler, in *Imperfections in III-V Materials, Semiconductors and Semimetals*, edited by E. R. Weber (Academic Press, New York, 1993), Vol. 38, Chap. 1, p. 1.
[19] K.J. Chao, A.R. Smith, and C.K. Shih, Phys. Rev. B **53**, 6935 (1996).

[20] Ph. Ebert, X. Chen, M. Heinrich, M. Simon, K. Urban, and M.G. Lagally, Phys. Rev. Lett. **76**, 2089 (1996).
[21] G. Schwarz, A. Kley, J. Neugebauer, and M. Scheffler, Phys. Rev. B **58**, 1392 (1998).
[22] Ph. Ebert, K. Urban, and M.G. Lagally, Phys. Rev. Lett. **72**, 840 (1994).
[23] A. Depuydt, N.S. Maslova, V.I. Panov, V.V. Rakov, S.V. Savinov, and C. Van Haesendonck, Appl. Phys. A: Mater. Sci. Process. **66**, S171 (1998).
[24] L.J. Whitman, J.A. Stroscio, R.A. Dragoset, and R.J. Celotta, Phys. Rev. B **42**, 7288 (1990); J. Vac. Sci. Technol. B **9**, 770 (1991).
[25] M. Alatalo, R.M. Nieminen, M.J. Puska, A.P. Seitsonen, and R. Virkkunen, Phys. Rev. B **47**, 6381 (1993).
[26] C.W.M. Castleton *et al.* (unpublished).
[27] A. Zylbersztejn, R.H. Wallis, and J.M. Besson, Appl. Phys. Lett. **32**, 764 (1978); L.K. Teles, L.M.R. Scolfaro, J.R. Leite, L.E. Ramos, A. Tabata, J.L.P. Castineira, and D.J. As, Phys. Status Solidi B **216**, 541 (1999).